Contents

1 Perturbation of the spin motion

The spin precession axis of a particle involved in betatron motion precesses about the stable invariant spin axis defined on the closed orbit (CO).

This precession can be observed in polarization data as a rapid, small-amplitude oscillation (example in Figure 2) on top of the *major effect* oscillation caused by the precession of spin about the CO axis. The frequency of this latter oscillation is used in the FD methodology as the EDM observable. It is estimated by fitting polarimetry data by a sine function. The rapid oscillations, therefore, constitute a model error.[1]

This model error will introduce a bias into the frequency estimate (the amplitude growth of the blue line oscillation in Figure 1 is due to the bias). In the following we investigate how this bias changes depending on the beam revolution direction, its stability over time, and the EDM estimate error introduced by it.

1.1 Simulation: Uniform beam

For simulation, we used an imperfect FS lattice, with E+B elements randomly tilted about the optical axis by angles picked from the normal distribution $N(4 \cdot 10^{-3}, 5 \cdot 10^{-4})$ [rad]. The systematic $\langle \Theta_{tilt} \rangle = 4 \cdot 10^{-3}$ radians was selected to ensure a sufficiently high radial precession rate, and hence reduce tracking time requirements. Tilts are simulated by applying a rotation matrix to the spin transfer map of the lattice as discussed in Section **??**. By doing it this way, we do not affect the orbital transfer map; that is, the closed orbit remains unchanged.

The beam was represented by an ensemble E of 4,000 rays, split into four groups of 1,000 rays: 1) rays offset from the CO at injection time in the x coordinate, 2) in the y cooridnate, 3) in both x and y, 4) in $d := \Delta K / K_0$. The x and y coordunates were uniformly sampled in the range ± 1 mm, d in the range $\pm 10^{-4}$. The reference energy $K_0 = 270.0092$ MeV (Frozen Spin energy for this lattice).

The beam polarization was computed from spin tracking data as

$$\boldsymbol{P} = \frac{\sum_{i \in E} \boldsymbol{s}_i}{|| \sum_{i \in E} \boldsymbol{s}_i ||}.$$

Then the vertical polarization component was fitted with the fit function $f = \sin(2\pi \cdot f \cdot t)$, with f the only fitted parameter. This procedure was carried out for the (identical at injection) CW and CCW revolving beams. We also estimated the reference rays' (CW & CCW) precession frequencies in the same way, by fitting the vertical spin component S_y^{CO} of the reference particle. The fit results are presented in Table 1. From this table, one can see that the polarization estimate is clearly biased toward the reference ray's estimate; however,

---

[1]A more sophisticated, for example autoregressive, model would solve this problem; however at a cost to precision.

the CW vs CCW estimates of either the reference ray or the polarization are statistically indistinguishable (assuming a normal distribution of the estimates, the hypothesis test for equality gives p-values of 30% and higher).
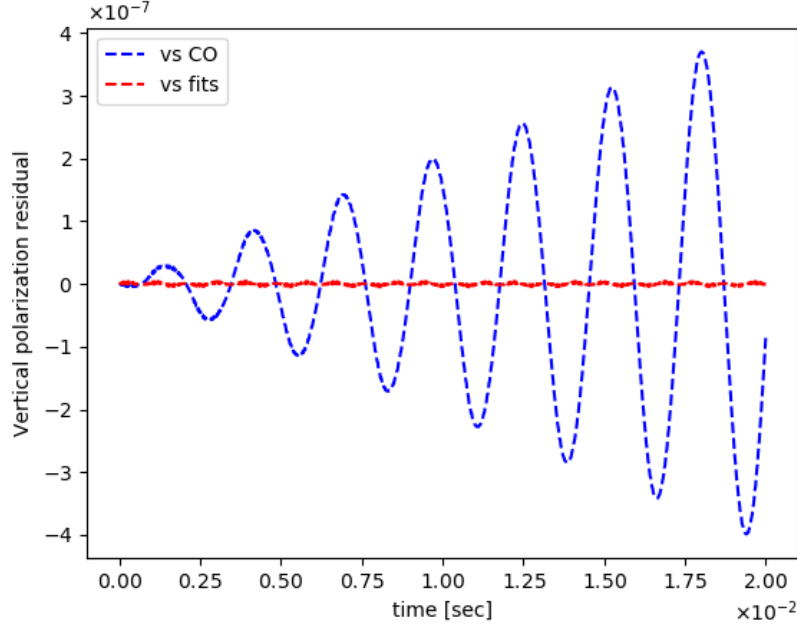

Figure 1: Vertical polarization residuals, computed as the difference between P_y (data) and: (red) $\hat{P}_y$ (model prediction), (blue) S_y^{co} (reference particle vertical spin component). The oscillations of the residuals are due to the rapid oscillations caused by the precession axis instability.

Table 1: Frequency estimates for the Uniform CW & CCW beams, reference ray and full beam, in Hz

Data		Polarization		Reference ray	
Frequency	Offset	CW	CCW	CW	CCW
Estimate	360.90365	$1.58 \cdot 10^{-7}$	$1.57 \cdot 10^{-7}$	$3.42902 \cdot 10^{-6}$	$3.42902 \cdot 10^{-6}$
SE	–	$1 \cdot 10^{-9}$	$2 \cdot 10^{-9}$	$5 \cdot 10^{-10}$	$5 \cdot 10^{-10}$

1.2 Simulation: Gaussian distribution beam

For this test we injected a beam of the same size, with x, y and d coordinates distributed normally (with standard deviations 1 mm, 1 mm, and 10^{-4} respectively). The coordinate distributions of the CW & CCW beams are presented
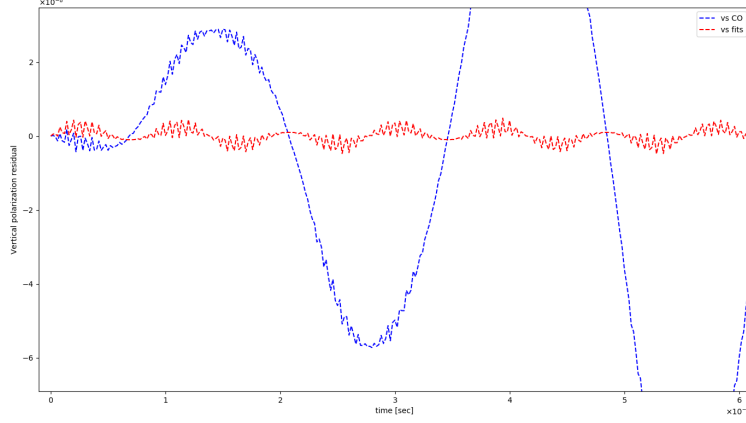
Figure 2: A zoom of Figure 1.

in Figures 3 and 4. As one can see, the beam's centroids are split by 0.004 mm in the horizontal direction, and 0.014 mm in the vertical direction. This split will have an effect on the resultant frequency estimate bias difference.

The fit results are summarized in Table 2.

Table 2: Frequency estimates for the Gaussian CW & CCW beams, reference ray and full beam, in Hz

Data		Polarization		Reference ray	
Frequency	Offset	CW	CCW	CW	CCW
Estimate	352.99403	$9.0405 \cdot 10^{-6}$	$7.792 \cdot 10^{-6}$	$4.149017 \cdot 10^{-5}$	$4.149017 \cdot 10^{-5}$
SE	$-$	$7 \cdot 10^{-10}$	$9 \cdot 10^{-9}$	$2 \cdot 10^{-11}$	$2 \cdot 10^{-11}$

The polarization frequency estimate difference

$$\varepsilon := \hat{f}_{CW} - \hat{f}_{CCW} = 1.249 \cdot 10^{-6} \pm 9 \cdot 10^{-9} \text{ [Hz]}.$$

One can see that the difference cannot be explained by statistical uncertainty.

Together with the uniform beam simulation, the above result drives the conclusion that the beam distribution asymmetry is a source of systematic error via spin precession axis direction variation. This systematic effect should reduce with the beam size, as in that case the coordinate distributions become more symmetrical.

Considering the last point, assume ε is proportional to the beam distribution centroid difference, defined by the coordinate distribution means. The expectation values of the coordinate distributions are located on the closed orbit, which is the same for the CW and CCW beams. The actual beam centroids
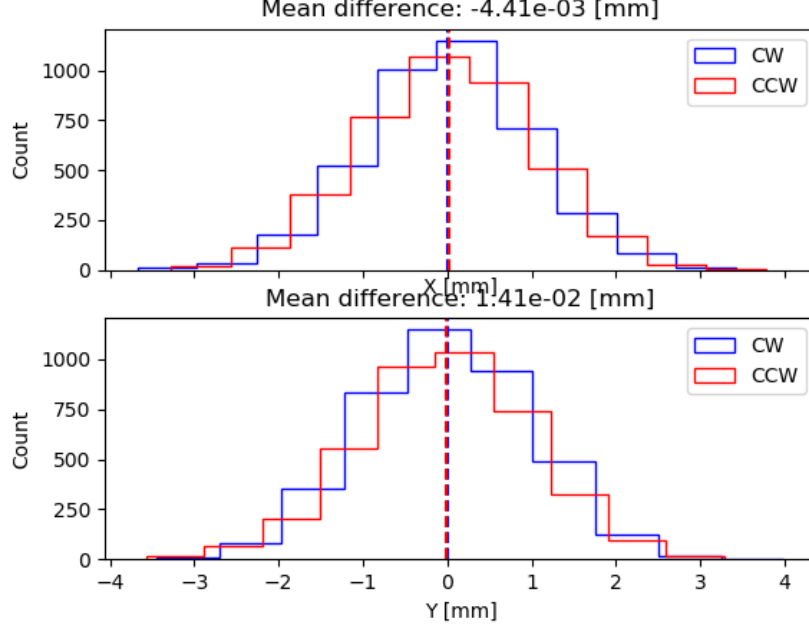
4

Figure 3: The x and y initial beam distributions.

are distributed about this point in a normal distribution with some standard deviation. Denote that standard deviation $\sigma_{mean} \equiv \sigma_{4k}$ for the beams used in the simulation above. This standard deviation gives us a frequency estimate variation on the order of 10^{-6} Hz (while the statistical uncertainty standard deviation is 10^{-9} Hz). The standard error of the mean is computed as

$$\sigma_{mean} = \frac{\sigma}{\sqrt{n}},$$

where n is the sample size, which in our case is the number of beam particles.

Now, if we used a $n = 4 \cdot 10^9$ particle beam instead of the $n = 4 \cdot 10^3$ one, we'd have $\sigma_{4b} = \sigma_{4k} \cdot 10^{-3}$. Assuming a linear relationship between the centroid difference and the frequency bias difference, the latter's standard deviation would reduce to 10^{-9}, which is then comparable with statistical error.

1.3 The effect of the beam distribution centroid difference on spin precession

Now we will test the hypothesis that the estimate bias difference is proportional to the beam centroid difference.

This time we repeated the test from the previous section for multiple (30) trials. We used the same imperfect lattice on each trial; trials only differ by
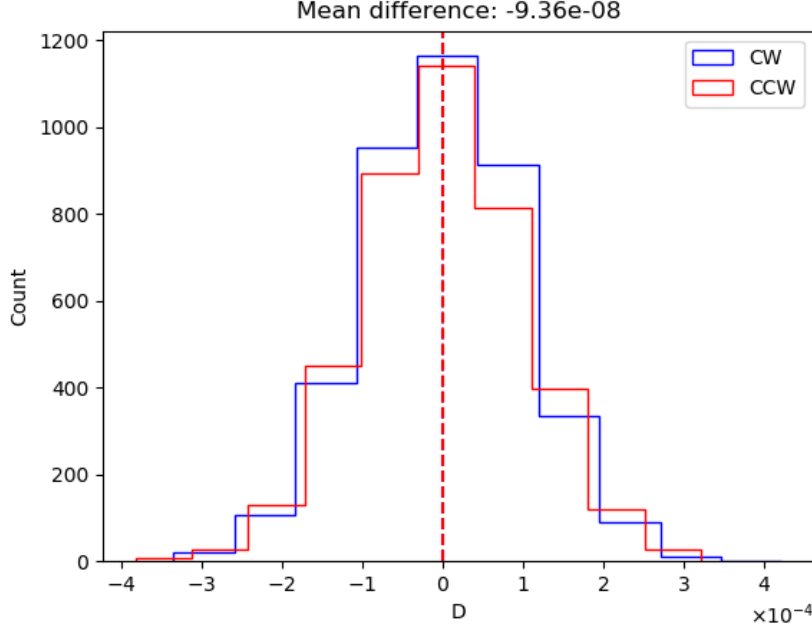
5

Figure 4: The d initial beam distributions.

their initial beam distributions. An example of the polarization oscillations in this lattice is given in Figure 5.

For each beam, we computed its centroid, defined as $\boldsymbol{c} = (\langle x_0 \rangle, \langle y_0 \rangle, \langle d_0 \rangle)$, and took the difference $\Delta \boldsymbol{c} := \boldsymbol{c}_i^{CW} - \boldsymbol{c}_i^{CCW}$ (i the trial number). We then regressed (non-weighted linear regression) ε_i on the components of $\Delta \boldsymbol{c}_i$. The results are plotted in Figure 6. We found a statistically significant dependence on the vertical centroid difference component (p-value $\approx 0\%$).

In order to make sure that the bias difference is not related to the change of the beam revolution direction, we checked the centroid difference dependence of the bias on the same direction beams. The dependence remains.

2 Spin decoherence in a perfectly aligned ring

Spin coherence refers to a measure or quality of preservation of polarization in an initially polarized beam. [1, p. 205]

When a polarized beam is injected into a storage ring, the spin vectors of the beam particles start precessing around the vertical (guiding) magnetic field. The precession frequency is dependent upon the equilibrium-level energy of the particle, which differs for the particles in the beam.

This does not pose a problem when the initial polarization is vertical; how-
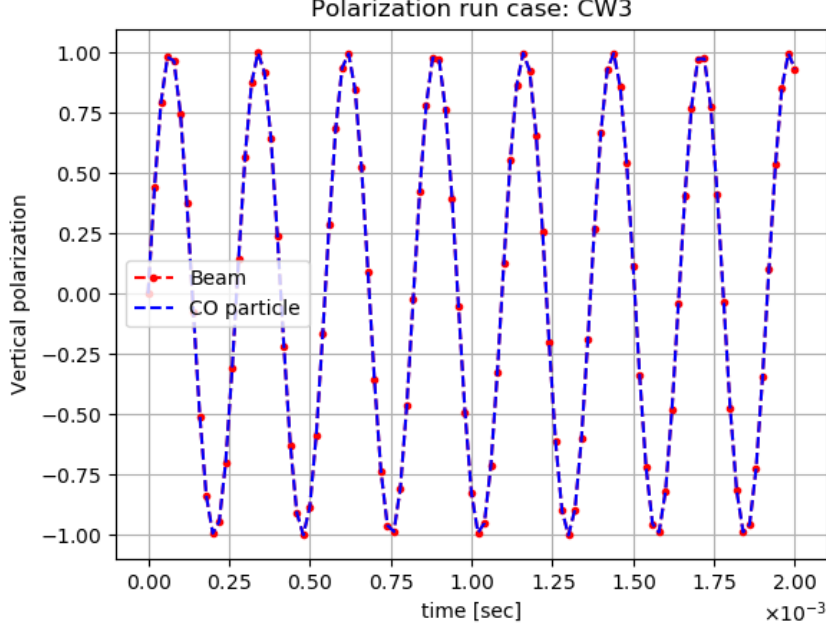
Figure 5: Example of polarization oscillations in the used lattice.

ever, the FS storage ring method requires spin polarization along the momentum vector, i.e., in the horizontal plane. Therefore, spin decoherence is an inherent weakness of the FS method.

2.1 Spin coherence time requirements

The spin coherence time (SCT) for an FS method performed in a perfectly aligned storage ring is determined by the smallest detectable angle by which the beam polarization vector is tilted from the horizontal plane by EDM alone. For the sensitivity level of 10^{-29} $e \cdot cm$ it is about $5 \cdot 10^{-6}$. [2]

According to the T-BMT equation,

$$\Omega_{EDM,x} = \eta \frac{qE_x}{2mc},$$

where η is the proportionality factor between the EDM and spin, equaling 10^{-15} for the deuteron, for the given EDM sensitivity limit. [1, p. 206]

For the deuteron BNL FS storage ring, $E_x = 12$ MV/m, [2, p. 19] and so $\Omega_{EDM,x} \approx 10^{-9}$ rad/sec. This gives an SCT of approximately 1000 seconds in order that the vertical polarization reaches a detectable level of 1μrad. [1, p. 207]

7

2.2 Origin of decoherence

Spin decoherence in a particle bunch is caused by the difference in the spin precession angular velocities, which, in turn, is due to the difference in the particles' orbit lengths and momentum values. This can be seen from the following considerations.

When a particle with spin enters a magnetic field area, the spin vector starts turning about the magnetic field vector with an angular velocity defined by the T-BMT equation (**??**):

$$\boldsymbol{\Omega}_{MDM} = \frac{q}{m} G \boldsymbol{B}.$$

Upon exiting the field area, the spin has turned by an angle

$$\theta = \Delta t \cdot \Omega_{MDM} = \frac{L}{v} \cdot \frac{q}{m} GB \cdot \frac{\gamma_0}{\gamma_0} = \frac{L\gamma_0 GB}{B\rho} = \frac{L}{\rho} \gamma_0 \cdot G,$$

where L is the path length inside the B-field, and $B\rho = p/q$ is the magnetic rigidity.

In the simple model considered so far, the influence of the orbital dynamics upon the spin dynamics is expressed by the $\gamma_0 L/\rho$ (effective gamma) term. In the case of the reference particle, $\gamma_0 L/\rho = \gamma_0 \alpha$, α is the bend angle, while for a particle involved in betatron motion, effective gamma is greater. In the following sections we will specify the connection between the spin and orbital dynamics of a particle further in a more general fashion.

2.2.1 Equilibrium momentum shift

The longitudinal dynamics of a charged particle on the reference orbit in a storage ring is described by the system of equations:

$$\begin{cases} \frac{d\varphi}{dt} &= -\omega_{RF}\eta\delta, \\ \frac{d\delta}{dt} &= \frac{qV_{RF}\omega_{RF}}{2\pi h\beta^2 E} \sin\varphi. \end{cases}$$

In the equations above: φ is the phase deviation from the reference $\varphi_0 = 0$; $\delta = \frac{\Delta p}{p_0}$ is the relative momentum deviation from the momentum p_0 of the reference particle; V_{RF}, ω_{RF} are the voltage and oscilation frequency of the RF field; $\eta = \alpha_0 - \gamma^{-2}$ is the slip factor, with α_0 being the compaction factor defined by $\Delta L/L = \alpha_0\delta$, and L being the orbit length; h is the harmonic number; E is the total energy of the accelerated particle. $\omega_{RF} = 2\pi h f_{rev}$, where $f_{rev} = T_{rev}^{-1}$ is the beam revolution frequency.

The solutions of this system form a family of ellipses in the (φ, δ) space, centered at $(0,0)$. However, if we consider a particle involved in betatron oscillations, and use a higher-order Taylor expansion of the compaction factor $\alpha = \alpha_0 + \alpha_1\delta$, the first equation of the system transforms into: [3, p. 2579]

$$\frac{d\varphi}{dt} = -\omega_{RF}\left[\left(\frac{\Delta L}{L}\right)_\beta + \left(\alpha_0 + \gamma^{-2}\right)\delta + \left(\alpha_1 - \alpha_0\gamma^{-2} + \gamma^{-4}\right)\delta^2\right],$$

8

where $\left(\frac{\Delta L}{L}\right)_\beta = \frac{\pi}{2L}\left[\varepsilon_x Q_x + \varepsilon_y Q_y\right]$, is the betatron motion-related orbit lengthening; ε_x and ε_y are the horizontal and vertical beam emittances, and Q_x and Q_y are the horizontal and vertical tunes. [3, p. 2580]

The solutions of the modified system are no longer centered at the same point. Orbit-lengthening and momentum deviation cause an equilibrium-level momentum shift [3, p. 2581]

$$\Delta\delta_{eq} = \frac{\gamma_0^2}{\gamma_0^2\alpha_0 - 1}\left[\frac{\delta_m^2}{2}\left(\alpha_1 - \alpha_0\gamma^{-2} + \gamma_0^{-4}\right) + \left(\frac{\Delta L}{L}\right)_\beta\right], \tag{1}$$

where δ_m is the amplitude of synchrotron oscillations.

2.2.2 Effective Lorentz factor

The equilibrium energy associated with the momentum shift (1), termed the *effective Lorentz factor*, is [4]

$$\gamma_{eff} = \gamma_0 + \beta_0^2\gamma_0 \cdot \Delta\delta_{eq}, \tag{2}$$

where γ_0, β_0 are the reference particle's Lorentz factor and normalized speed. Equations (1) and (2) define the link between the particle spin and orbital dynamics.

2.3 Sextupoles for the reduction of decoherence

To minimize the spin decoherence dur to betatron motion and momentum deviation, sextupoles (or octupoles) may be used [1, p. 212]

A sextupole of strength

$$S_{sext} = \frac{1}{B\rho}\frac{\partial^2 B_y}{\partial x^2},$$

where $B\rho$ is the magnetic rigidity, affects the first-order compaction factor as [3, p. 2581]

$$\Delta\alpha_{1,sext} = -\frac{S_{sext}D_0^3}{L}, \tag{3}$$

and simultaneously the orbit length as

$$\left(\frac{\Delta L}{L}\right)_{sext} = \mp\frac{S_{sext}D_0\beta_{x,y}W_{x,y}}{L}, \tag{4}$$

where $D(s,\delta) = D_0(s) + D_1(s)\delta$ is the dispersion.

In the following sections, we will call the decoherence accociated with horizontal/vertical betatron, and synchrotron oscillations, respectively X-/Y-, and D-decoherence.

It can be observed from eqs equations (3, 4), that three sextupole families are required for the reduction of decoherence, placed in the maxima of: β_x, $beta_y$ for the reduction of X-,Y-decoherence, and D_0 for D-decoherence.

2.3.1 Simulation

In order to check the effectiveness of the sextupole method for the suppression of decoherence, a simulation was carried out using the COSY INFINITY code.

We took a perfectly aligned FS lattice, with three families of sextupoles (SX, SY, SD) placed as was explained at the end of section 2.3. Then we varied the strengths of each sextupole family (GSX, GSY, GSD) individually, and computed the spin tunes of particles offset at injection from the reference particle in: *a)* the x-coordinate for the SX-family, *b)* y-coordinate for the SY-family, and *c)* $d = \Delta K / K_0$ for the SD-family.

The spin tune depends parabolically for each direction of offset:

$$\mu(x, y, d) = \mu_0 + \mu_{xx}x^2 + \mu_{yy}y^2 + \mu_{dd}d^2 + O(x^3) + O(y^3) + O(d^3).$$

The search for the optimal sextupole strengths was done in two iterations:

1. first, we manually varied the strengths in a wide range, and observed the flattening of the spin tune curve;

2. when the global minima were found approximately, we continued the optimization automatically (for each family independently), using the second-order Taylor expansion coefficient before the corresponding coordinate.

The simulation results at 300 MeV (30 MeV above the FS energy) are presented in Figure 7. After the optimization of the sextupole strengths, spin tune shows almost no dependence on the variable offsets.[2]

3 Fake signal simulation

Systematic errors due to imperfections in the physical lattice, including optical element misalignments, are causative to a fake EDM signal. [1, p. 230] Rotational misalignments are particularly problematic, since they induce the horizontal magnetic error field components B_x and B_z both of which rotate spin in the vertical plane, thus causing a fake EDM signal.

Analytical estimates of the MDM precession frequency about the radial axis were made by Senichev. [4] From the T-BMT equation, and the expression for the Lorentz force, the MDM precession rate about the radial axis is

$$\sigma\left[\Omega_x^{MDM}\right] = \frac{q}{m\gamma}\frac{G+1}{\gamma}\frac{\sigma\left[B_x\right]}{\sqrt{n}}, \tag{5}$$

where n is the number of tilted spin rotators, and $\sigma\left[B_x\right] = B_y\sigma\left[\delta h\right]/L$, $\sigma\left[\delta h\right]$ being the alignment error standard deviation. At alignment error $\sigma\left[\delta h\right] = 100\mu$m, and deflector length $L = 1$m, $\sigma\left[\Omega_x^{MDM}\right] \approx 100$ rad/sec. [4]

We studied spin dynamics in the FS and QFS lattices in the presence of rotational magnet misalignments using the COSY INFINITY code. Our simulations appear to confirm the above analysis.

---

[2]We were unable to suppress all three types simultaneously in this lattice. Specifically, when the SD-type sextupoles are turned on, the D-decoherence is suppressed as before, but the X- and Y-types degrade even further.

3.1 Error field implementation

In implementing field imperfections we followed the recommendations given in [1, p. 235]. A small perturbation of the magnetic field acts with a first-order perturbation correction as a small proportional rotation on the spin vector. Therefore, we implemented rotational magnet misalignments as an augmentation of the rotated elements with small, normally-distributed spin kicks.

According to eq (**??**), the MDM precession frequency change associated with an introduced error field $(B_x, 0, B_z)$ is

$$\Delta\Omega_{MDM} = \frac{q}{m}(B_x, 0, B_z),$$

so the spin kick angle is

$$\Theta_{kick} = t_0 \Delta\Omega_{MDM},$$

where $t_0 = L/v_0$ is the time-of-flight of the reference particle through the element.

3.2 Simulation

We randomly assigned tilt angles Θ_{tilt} to E+B elements in the FS lattice. The experiment was performed 11 times; each time the angles were selected from a normal distribution $N(\mu_0 \cdot (i - 5), \sigma_0)$, where $\mu_0 = 10 \cdot \sigma_0 = 10^{-4}$ rad, $i \in \{0, \ldots, 10\}$. After the construction of the 3rd order transfer map for the imperfect lattice, the spin tune and spin precession axis (SPA) Taylor expansions were computed. We then took the zero-order terms of the maps, representing the spin tune and SPA of the reference particle. The results are presented in Figure 8. In Figure 9 are shown the results when three pairs of E+B elements are rotated by opposite angles, and one element is rotated by an angle $\mu_i = (i - 5) \cdot 10^{-6}$ rad, $i \in \{0, \ldots, 10\}$. The simulations were done at 270.0092 MeV.[3]

References

[1] Eremey Valetov. FIELD MODELING, SYMPLECTIC TRACK-ING, AND SPIN DECOHERENCE FOR EDM AND MUON G-2 LATTICES. Michigan State University. Michigan, USA;. Available from: http://collaborations.fz-juelich.de/ikp/jedi/public_files/theses/valetovphd.pdf.

[2] D Anastassopoulos, V Anastassopoulos, D Babusci. AGS Proposal: Search for a permanent electric dipole moment of the deuteron nucleus at the

---

[3]At this energy the spin precession axis and spin tune are undefined in the beamline coordinate system used by COSY INFINITY in the perfect lattice. This corresponds to the situation when spin does not precess in any plane (horizontal or vertical), which is the FS condition in a perfect lattice.

10^{-29} $e \cdot cm$ level. BNL; 2008. Available from: `https://www.bnl.gov/edm/files/pdf/deuteron_proposal_080423_final.pdf`.

[3] Senichev Y, Zyuzin D. SPIN TUNE DECOHERENCE EFFECTS IN ELECTRO- AND MAGNETOSTATIC STRUCTURES. In: Beam Dynamics and Electromagnetic Fields. vol. 5. Shanghai, China: JACoW; 2013. p. 2579–2581. OCLC: 868251790. Available from: `https://accelconf.web.cern.ch/accelconf/IPAC2013/papers/wepea036.pdf`.

[4] Yury Senichev. Frequency domain method of the search for the deuteron electric dipole moment in a storage ring with imperfections;. Available from: `https://mail-attachment.googleusercontent.com/attachment/u/0/?ui=2&ik=7fc6107b60&view=att&th=15d604450498d398&attid=0.1&disp=safe&zw&saddbat=ANGjdJ8kSdMTQUkpPWe6xjODjjLdP-xU7StU6dUW7RLGZ3yMcRO6cF3dymVY89FbIIJLxgcHSSJLgWX4iK_XfdvgOGSJyuav2kRjMKdvRL4Hb-NZqtKdC2SQlsMFlwwJlI_vSCXwew-6R9HRaBMjVsRreHlULw3i9QtPOlzMGXHwGH4Mf0JkdGhwYfxhpI6WStzajdQibfA0oFRyEl861YacE3H4` `7HPH7gIk-qt2wNCgq-Vc6F97QozjqLYPeRq0SfxkALLCGJlhF1kJP3p9eL9fKbOqTl5JW2gZl-kEJvh5GWnJ-Eha` `DPcMW7JZNAi1hUqNUJ25jZTWB3PTdsaXUpkD-tMav1RHODj5hBK9zJhonZmtxX4R6vZ1SqEv-myKWFeS7NBZ1gY5`
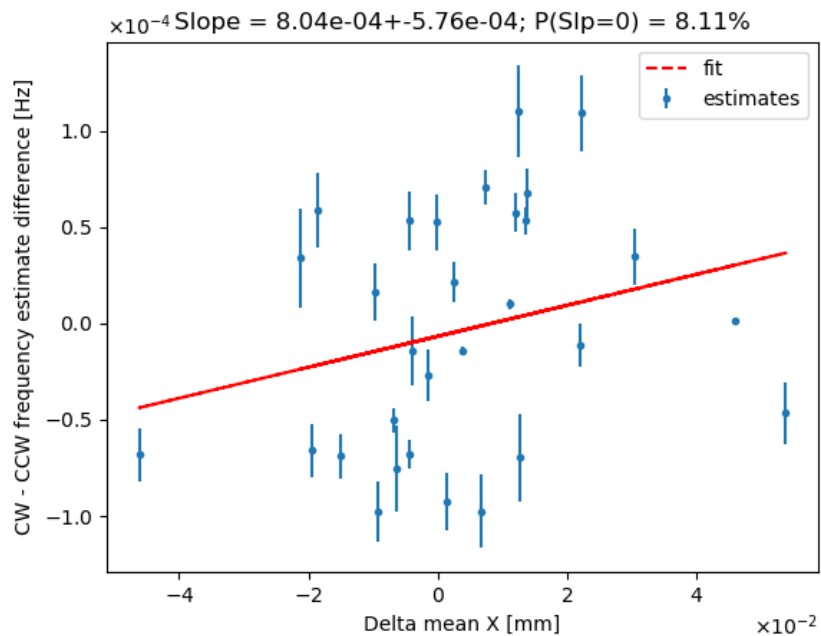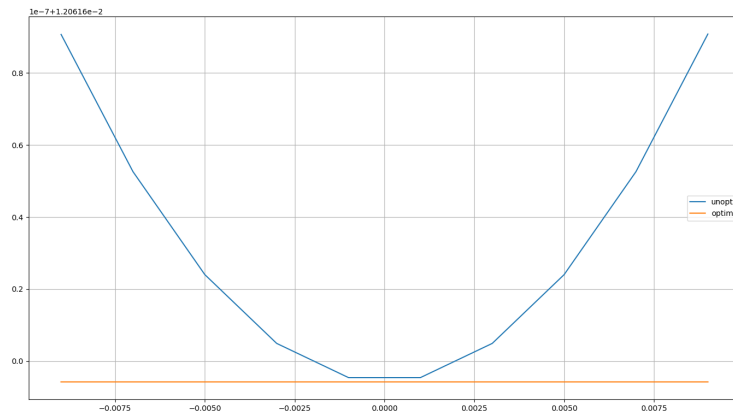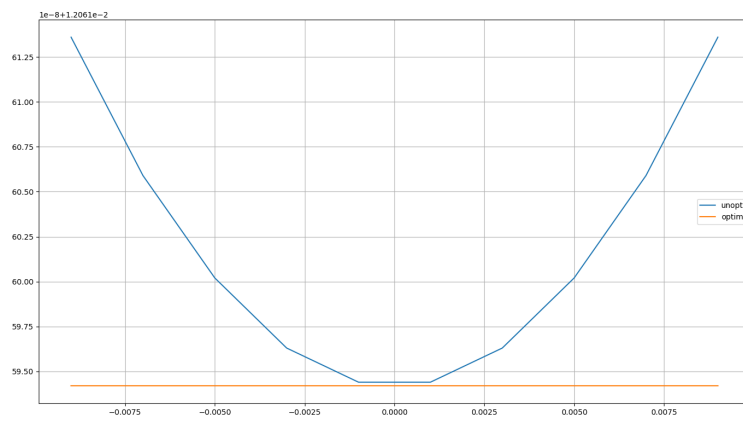
(a) The x coordinate.
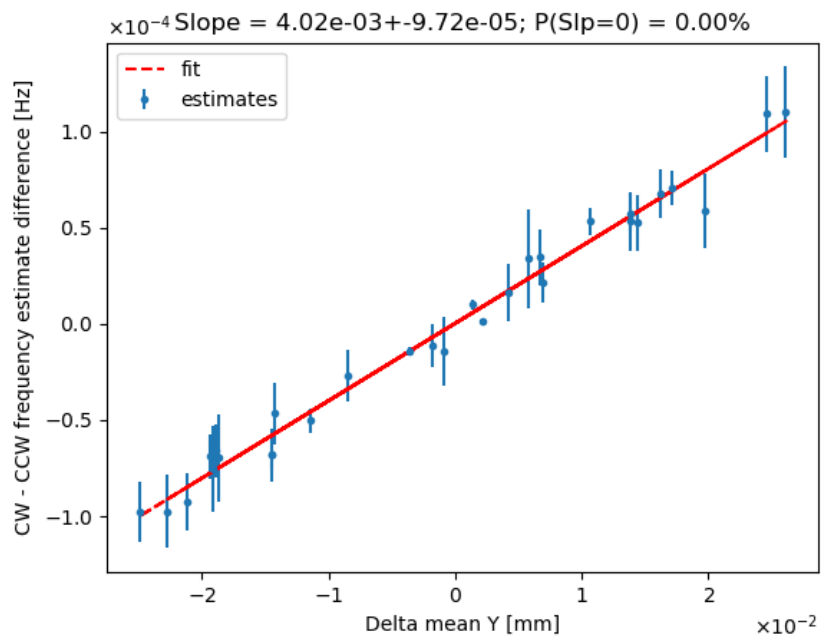
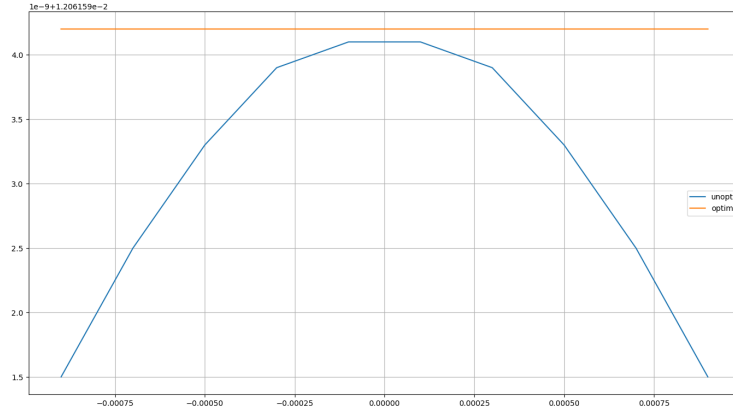(b) The y coordinate.
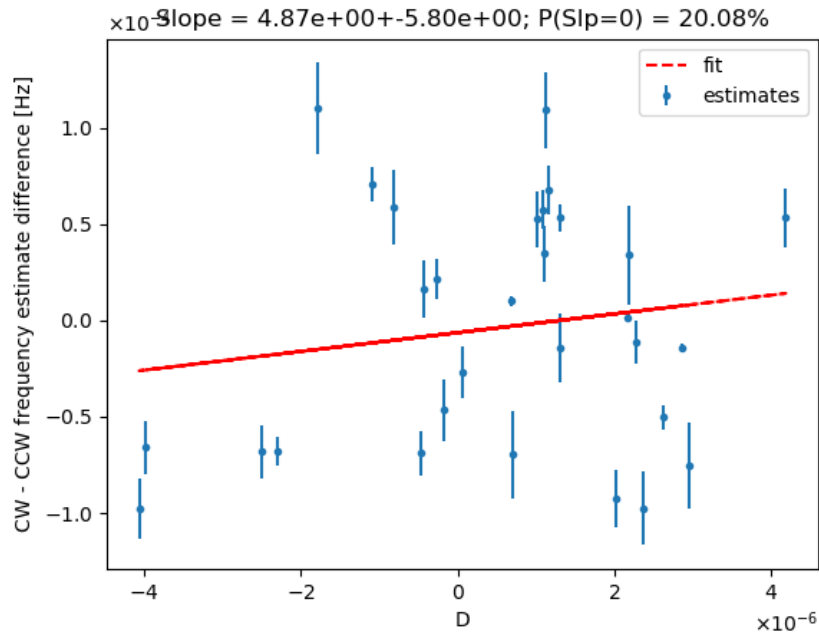
(c) The d coordinate.

Figure 6: Frequency estimate difference vs a beam centroid split coordinate.

(a) GSX optimized for the X bunch

(b) GSY optimized for the Y bunch

15

(c) GSD optimized for the D bunch

Figure 7: Spin tunes of offset particles vs the offsets, at 300 MeV, with/out the corresponding sextupole.
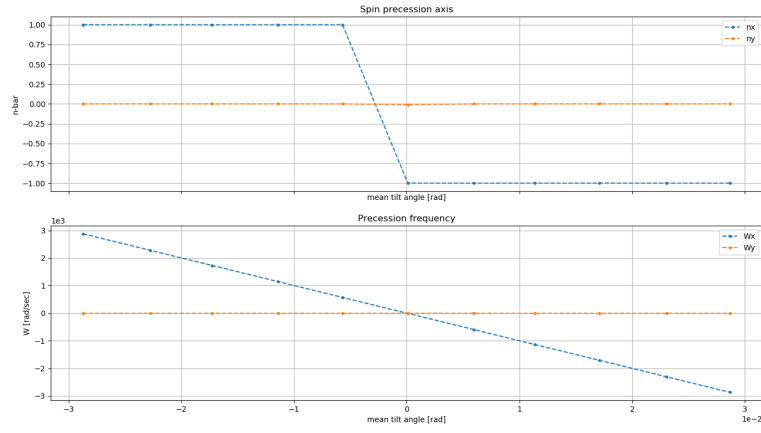

Figure 8: Spin precession axis and precession frequencies for the imperfect FS lattice, under the rotation of E+B elements.
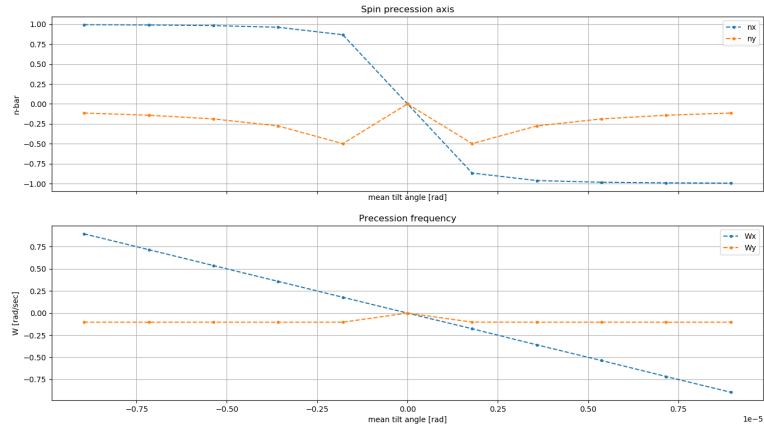
Figure 9: Three pairs of oppositely rotated E+B elements, plus an uncompensated element.